



## Ground stability of ellipsoidal cavity due to pipeline defects

Jim Shiau<sup>a,\*</sup>, Pak Cheong Leung<sup>a</sup>, Suraparb Keawsawasvong<sup>b</sup>, Sorawit Seehavong<sup>b</sup>,  
Jun Sugawara<sup>c</sup>

<sup>a</sup> School of Engineering, University of Southern Queensland, Toowoomba, QLD 4350, Australia

<sup>b</sup> Department of Civil Engineering, Thammasat School of Engineering, Thammasat University, Pathumthani 12120, Thailand

<sup>c</sup> Department of Transport and Main Roads, Queensland, 398 Tingira St, Bulwer Island, QLD 4008, Australia

### ARTICLE INFO

#### Keywords:

Sinkhole  
Stability analysis  
Cavity  
Limit analysis  
Collapse  
Blowout

### ABSTRACT

The problem of road-related sinkhole stability has long been one of the main safety concerns to pavement engineers. Collapse and blowout failures are two typical types of pipeline-related sinkhole failures. Although much research on sinkhole stability analyses can be found in the literature, most of them assume a simple circular or rectangular shape of a cavity. In this study, the problem of sinkhole stability in an ellipsoidal cavity is investigated under both blowout and collapse conditions using advanced finite element limit analysis with adaptive meshing in an axisymmetric condition. A dimensionless pressure ratio is defined to represent sinkhole stability that is a function of many design parameters such as depth ratio, elliptical shape ratio, and soil strength ratio. Selected results are compared with published solutions, and comprehensive solutions of the parametric study are presented in the form of charts for use by design engineers. The present study contributes to the understanding of sinkhole stability under an ellipsoidal cavity, and it should be of interest to the road engineering community.

### 1. Introduction

Road-related sinkholes caused by damaged water mains have increased dramatically in recent decades due to global climate changes. Consequently, road subsidence and sinkhole collapses have become one of the major research problems in geotechnical and road engineering. Scientific research is undergoing in relation to road-related sinkholes caused by broken water mains since it is a serious threat in many countries throughout the world (Gutiérrez et al., 2014). Table 1 presents a list of recent sinkhole occurrences worldwide. According to Ali and Choi (2019), the lack of maintenance, increasing water pressure, differential settlement, root damage, and corrosion are some of the reasons that contribute to water main damage. The problem needs to be better understood, given the current rise in sinkhole incidents.

Sinkholes can develop when subsurface soil erosion creates a soil hollow. At the ground's surface, circular sinkhole formations are the most common. The various stages of soil failures associated with water mains are conceptually illustrated in Fig. 1. The limit loads acting on the upward and downward orientations of the sinkhole are the triggers for the passive (blowout) and active (collapse) failures. Low pipe pressure causes the loose soil particles to be dragged into the sewer pipe through the pipe's crack, leaving a hole in the ground. On the other hand,

blowout failure can be caused by high water pressure (Indiketiya et al., 2019). Therefore, it is hypothesized that the beginning of a cavity is brought on by a fracture in the pipe (Shiau et al., 2021a).

It is well known that the shape of an underground cavity is complex and cannot be predicted due to its progressive failure nature. Therefore, standard geometries for the cavities were often used for various geotechnical stability examples caused by pipe leakage (Shiau et al., 2021a). The two primary types of trapdoor failures are collapse failure (downward movement) and blowout failure (upward movement). Two important factors that contribute to collapse failures are the self-weight of the soil mass and ground surcharge pressures, whereas blowout failures are exclusively caused by external forces acting against the soil weight and ground surcharge, such as the water main pressure (Shiau et al., 2021a). Several studies have been reported on "collapse" stability, with most considerations given to a flat planar trapdoor. Very few studies can be found in relation to blowout stability.

Sloan et al. (1988a,1988b) examined the stability of flat planar trapdoors under active plain strain conditions. This is one of the important early works associated with "collapse" analysis. In recent years, Shiau et al. (2021a,2021b;2022a) investigated pipeline burst-related ground stability above a broken water main pipeline under three modelled stages of internal soil erosion. The study suggested

\* Corresponding author.

E-mail address: [jim.shiau@usq.edu.au](mailto:jim.shiau@usq.edu.au) (J. Shiau).

<https://doi.org/10.1016/j.apples.2023.100163>

Received 24 October 2023; Accepted 6 November 2023

Available online 9 November 2023

2666-4968/© 2023 The Authors. Published by Elsevier Ltd. This is an open access article under the CC BY-NC-ND license (<http://creativecommons.org/licenses/by-nc-nd/4.0/>).

**Table 1**  
Recent cases of sinkhole events with causes and effects.

Time	Location	Cause	Effect	Reference
Mar 2022	Brisbane, Australia	Flooding	Road Damage	<a href="#">Brisbane times, 2022</a>
Jul 2022	Rotorua, New Zealand	A geothermal hole opened up	Footpath damage, injuries of two tourist	<a href="#">9News, 2022</a>
Aug 2022	Atacama, Chile	Mining activities, collapse after all the mineral is extracted	The deepest sinkhole in the world with 656 feet depth and 105 feet width	<a href="#">The Watchers, 2022</a>
Sep 2022	Villa Nueva, Guatemala	Sewer breakage	Road damage, swallowed one car and two people missing	<a href="#">9News, 2022</a>
Sep 2022	Perth, Australia	Water main breakage	Swallowed one car	<a href="#">7 News, 2022</a>
Sep 2022	Sydney, Australia	Water and Sewage pipes burst	Road damage with 10 m wide hole	<a href="#">9News, 2022</a>
Oct 2022	San Francisco, United States	Water main breakage	Road Damage	<a href="#">San FranciscoChronicle, 2022</a>

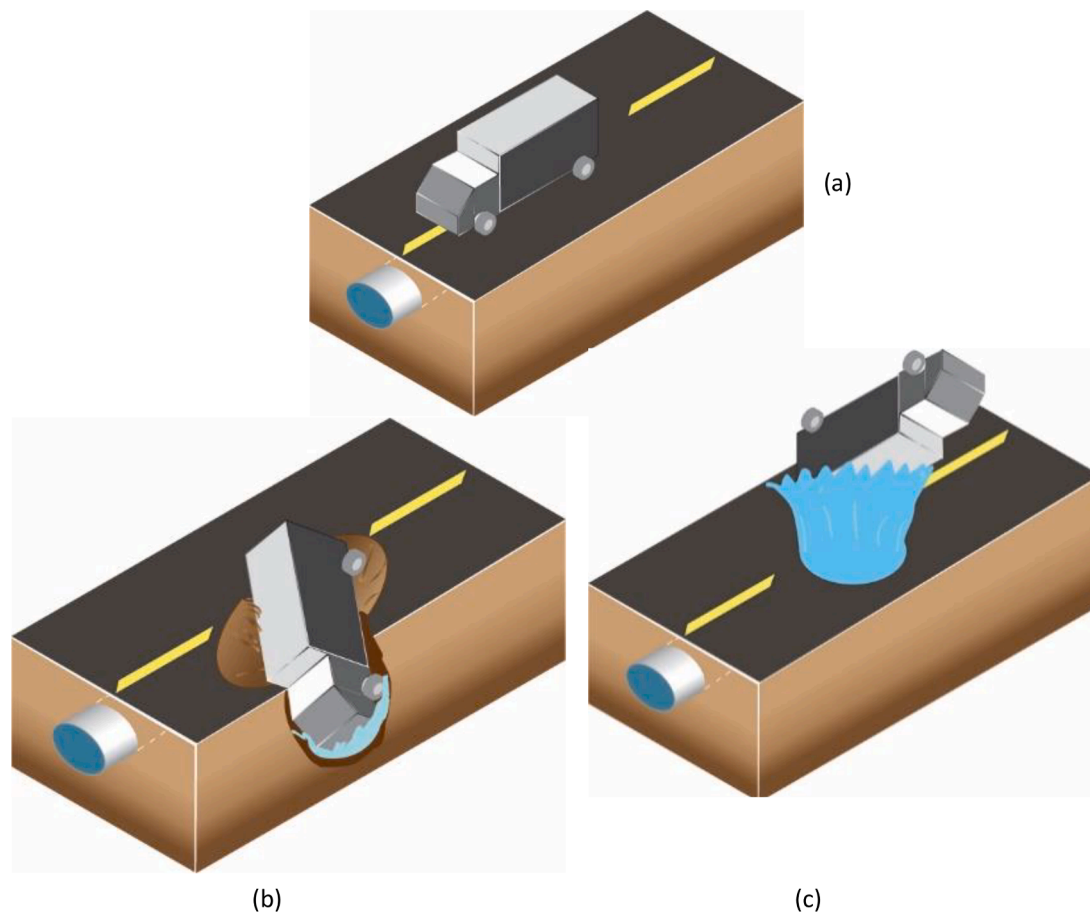


**Fig. 1.** Illustration of various stages of water main related soil failures: (a) Initial stage; (b) Collapse; (c) Blowout.

further investigation on the stability of sinkholes under axisymmetric conditions for the blowout stability impact due to changes of elliptical cavity shape. [Dutta and Bhattacharya \(2021\)](#) used lower-bound finite element limit analysis with second-order conic programming to investigate the stability of dual elliptical tunnels in soft clay. [Yang et al. \(2019\)](#) used the upper-bound finite element method and rigid translatory moving elements in cohesive frictional soils to examine the effects of surcharge loading on an elliptical tunnel. Using an upper-bound solution technique, [Zhang et al. \(2018\)](#) examined the stability of elliptical tunnels in cohesionless soils. Additionally, the finite element upper-bound approach with the plastic deformation element method was used to study the stability analysis of an unlined elliptical tunnel.

Noting that most earlier studies focused on the basic trapdoor shapes

of the circular, square, and rectangular ([Ukritchon et al., 2019](#); [Shiau et al., 2021c](#); [2022b-c](#); [Shiau and Hassan, 2020](#); [2021](#); [Keawsawasvong and Shiau, 2022](#); [Keawsawasvong and Likitlersuang, 2020](#); [Keawsawasvong and Ukritchon, 2019](#)), there have not been many studies on elliptical shape modification. Whereas sinkhole incidents are frequently observed on roads, there has also been a lack of studies in relation to sinkhole stability above the pressurized water supply mains. This paper thus presents a novel study by investigating the sinkhole stability of ellipsoidal cavities in an axisymmetric condition. [Fig. 2](#) shows such a 3D problem in axisymmetric conditions. Finite element limit analysis (FELA) and adaptive mesh technique are adopted to study the stability of sinkholes in both collapse and blowout conditions. The statement of the problem considered in the study scope is presented next.

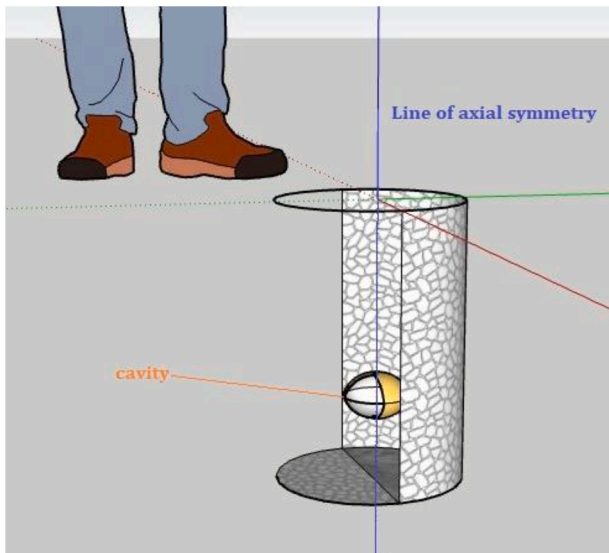


Fig. 2. 3D Illustration of an ellipsoidal cavity in axisymmetric condition.

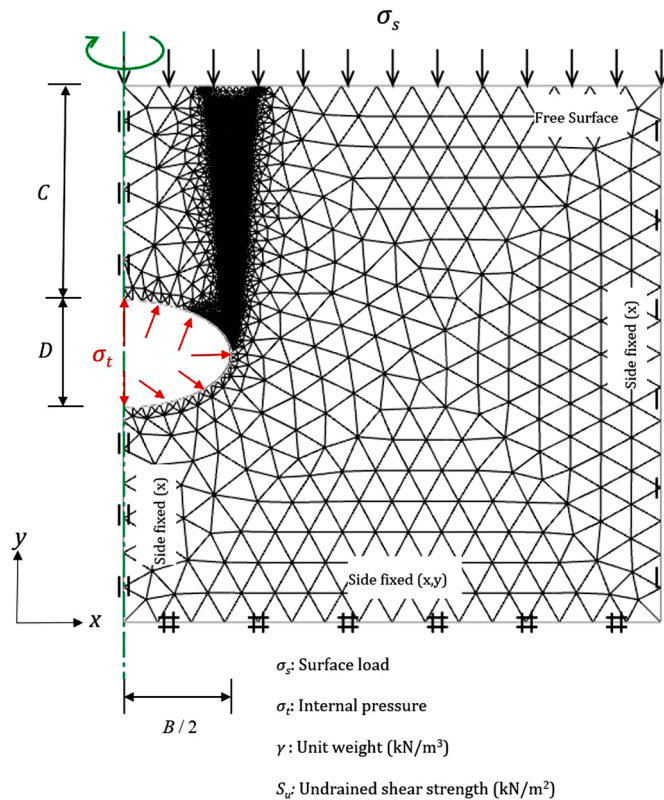


Fig. 3. Problem definition and FELA mesh ( $B/D = 2$ ).

## 2. Problem definition

The equation of a standard ellipse centred at the origin with width  $2a$  and height  $2b$  is shown in Eq. (1). For an ellipsoidal cavity shape in axisymmetric condition, Eq. (1) can be used to describe its geometry.

$$\frac{x^2}{a^2} + \frac{y^2}{b^2} = 1 \quad (1)$$

where  $a = B/2$ ,  $b = D/2$  and  $x$  and  $y$  are the coordinates of an ellipse. Using Eq. (1), examples of adaptive FELA mesh are shown in Figs. 3 and

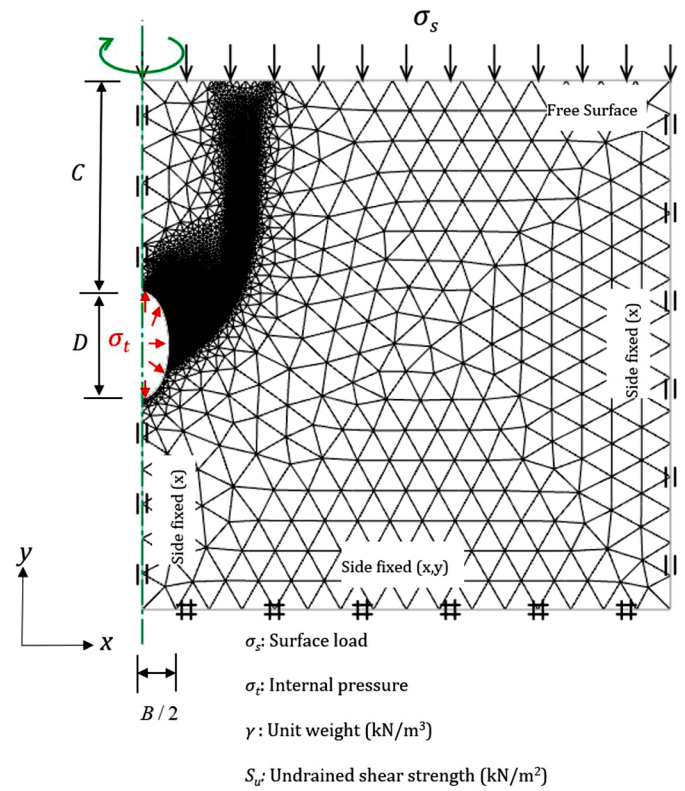


Fig. 4. Problem definition and FELA mesh ( $B/D = 0.5$ ).

4 for width-to-height ratios ( $B/D$ ) of 2 and 0.5, respectively. The cavities in both instances have a cover ( $C$ ), depth ( $D$ ), and width ( $B$ ). The ground surface is subjected to a surface pressure ( $\sigma_s$ ), whereas the inner perimeter of the opening is exposed to a pressure ( $\sigma_t$ ). With a soil unit weight of  $\gamma$  and an undrained shear strength of  $S_u$ , the soil is considered as a rigid-perfectly plastic Tresca material, which is the same as a Mohr-Coulomb material with zero soil frictional angle.

Terzaghi (1936) used the experimental investigation of stress on sand to define active trapdoor failure. The terminology used in the active mode is due to the surcharge stress ( $\sigma_s$ ) and the self-weight pressure ( $\gamma H$ ) whereas the passive mode is a result of an uplifting pressure ( $\sigma_t$ ) that simulates cavity blowout failure. The soil stability of the underground cavity was further investigated by Broms and Bennermark (1967) in the laboratory, and the stability number in Eq. (2) is recommended for the evaluation of undrained stability.

$$\text{Stability number, } (N) = \frac{\sigma_s - \sigma_t + \gamma H}{S_u} \quad (2)$$

where  $S_u$  is undrained shear strength,  $\gamma$  is the unit weight of the soil, and  $H$  is soil cover depth.

In contrast to Broms and Bennermark (1967), Davis et al. (1980) employed kinematic upper bound analysis for the stability problem. They expressed the pressure ratio ( $PR$ ) as the stability number, which is dependent on the ratios of depth and soil strength. Following Davis's approach, Eq. (3) is used to express the stability of the ellipsoidal cavity problem in this paper.

$$PR = \frac{\sigma_s - \sigma_t}{S_u} = f\left(\frac{C}{D}, \frac{B}{D}, \frac{\gamma D}{S_u}\right) \quad (3)$$

where  $C$  is the cover to the crest of the cavity,  $D$  is the depth of the cavity,  $B$  is the width of the cavity,  $S_u$  is undrained shear strength, and  $\gamma$  is the unit weight of soil. Eq. (3) shows that the stability is independent of the loading direction in undrained clay with zero internal frictional angle, and the pressure ratio in this equation is found to be less complicated

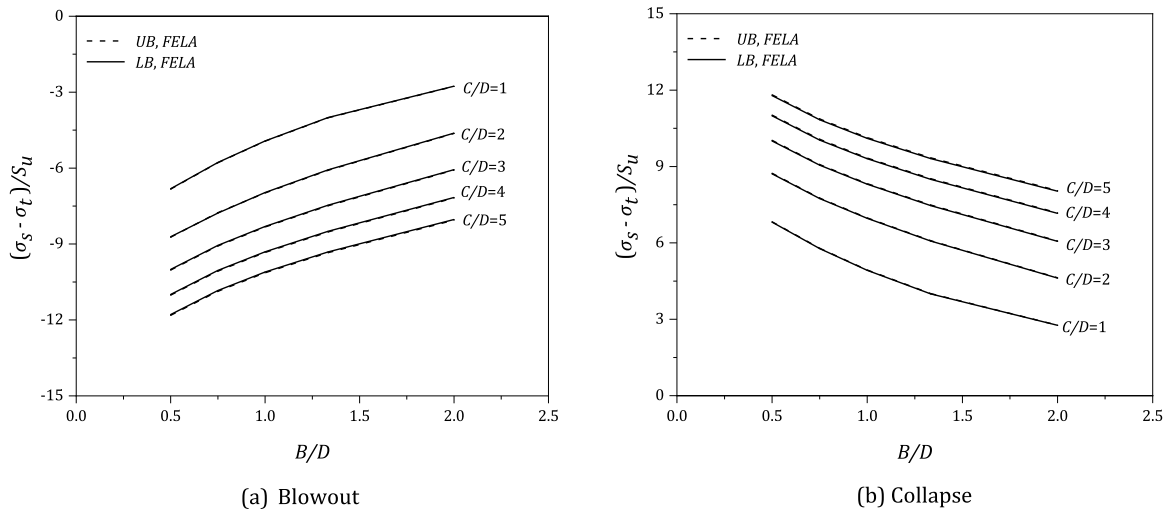


Fig. 5.  $(\sigma_s - \sigma_t)/S_u$  vs  $(B/D)$  for various  $(C/D)$  -  $\gamma D/S_u = 0$ .

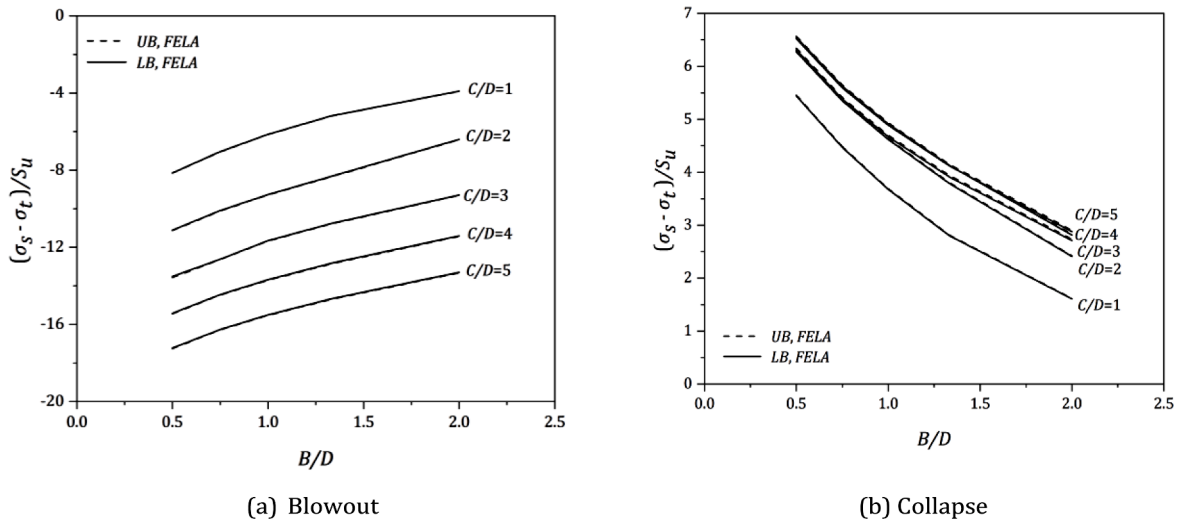


Fig. 6.  $(\sigma_s - \sigma_t)/S_u$  vs  $(B/D)$  for various  $(C/D)$  -  $\gamma D/S_u = 1$ .

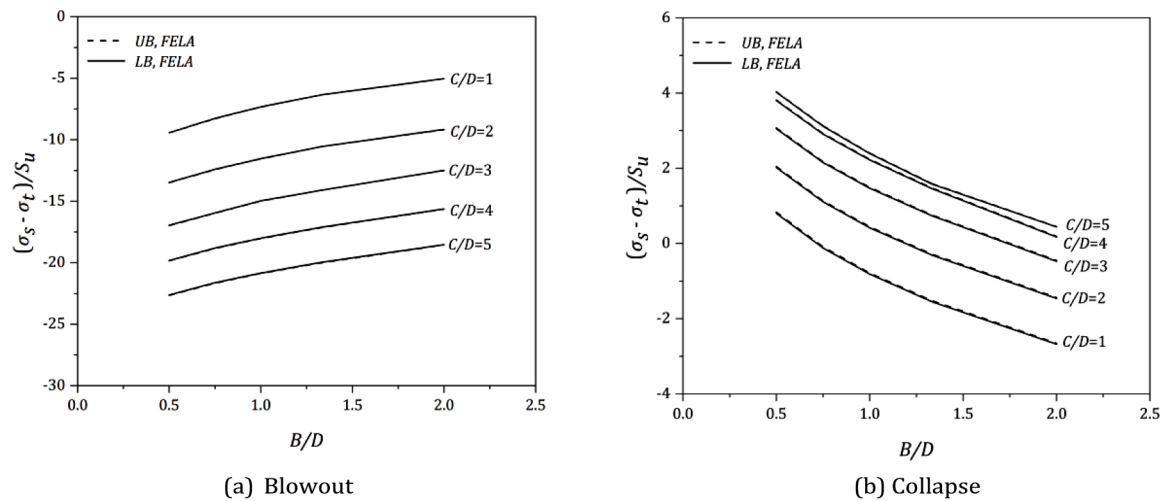


Fig. 7.  $(\sigma_s - \sigma_t)/S_u$  vs  $(B/D)$  for various  $(C/D)$  -  $\gamma D/S_u = 2$ .

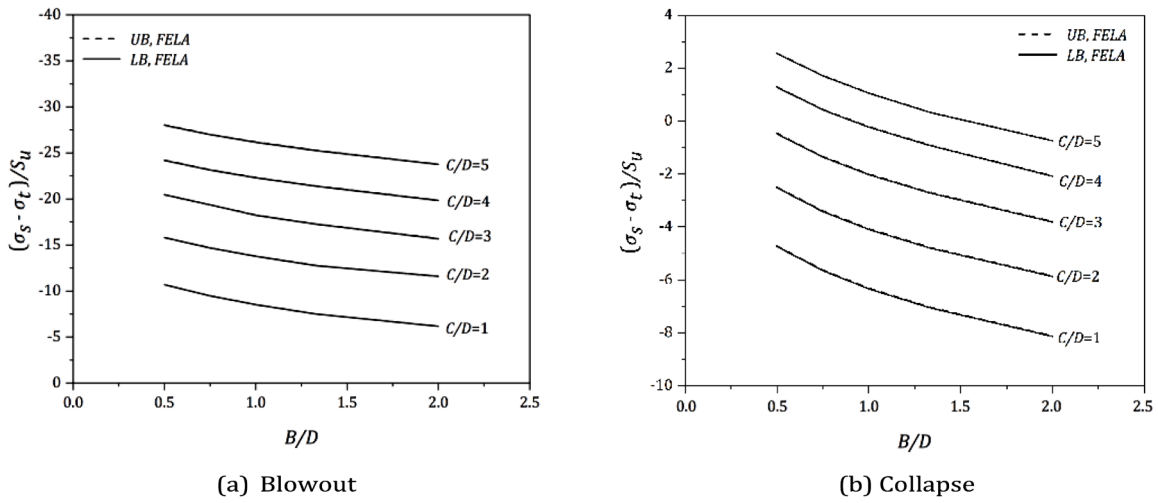


Fig. 8.  $(\sigma_s - \sigma_t)/S_u$  vs  $(B/D)$  for various  $(C/D)$  -  $\gamma D/S_u = 3$ .

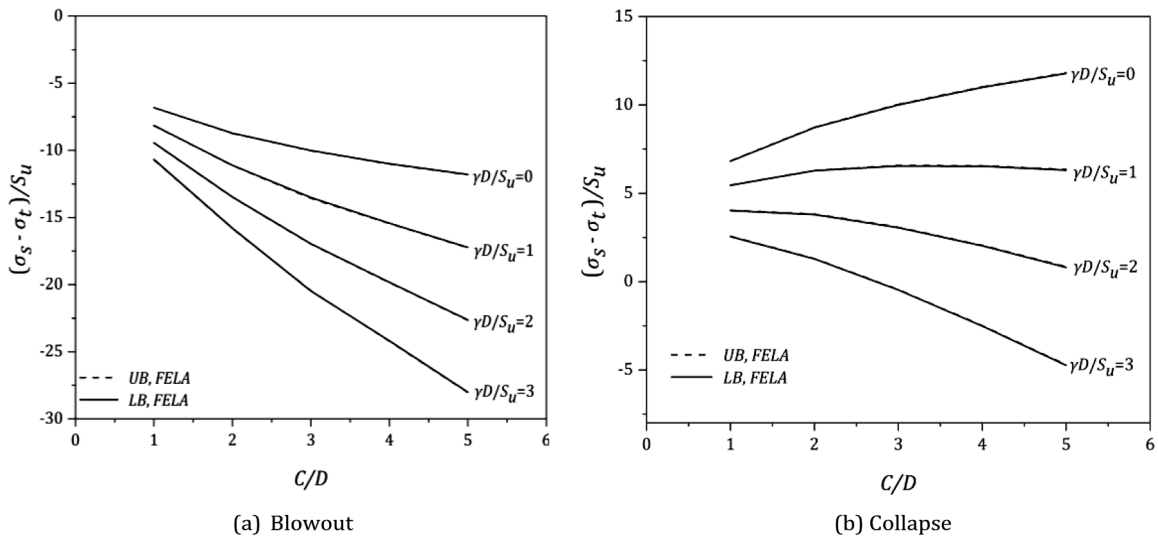


Fig. 9.  $(\sigma_s - \sigma_t)/S_u$  vs  $(C/D)$  for various  $(\gamma D/S_u)$  -  $B/D = 0.5$ .

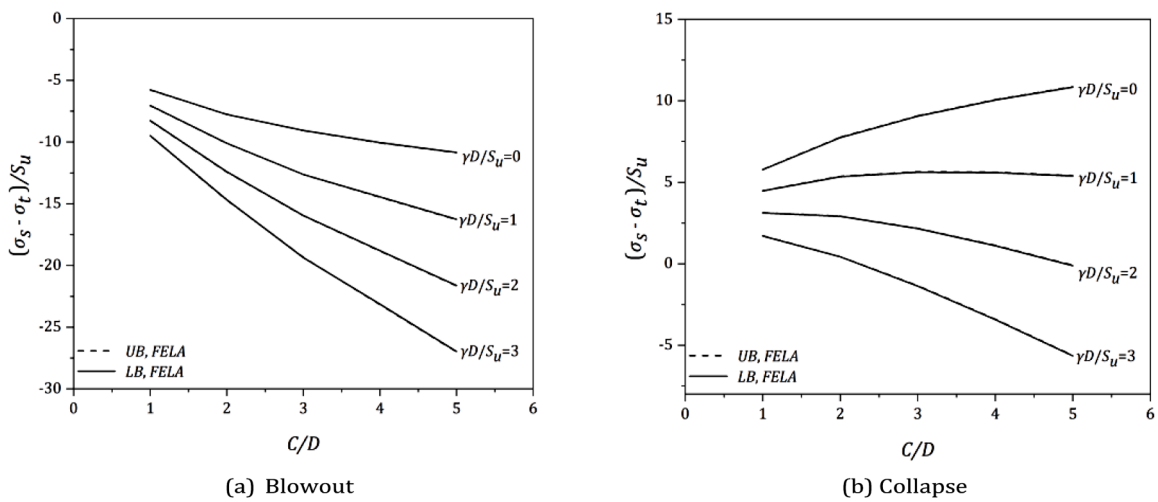


Fig. 10.  $(\sigma_s - \sigma_t)/S_u$  vs  $(C/D)$  for various  $(\gamma D/S_u)$  -  $B/D = 0.75$ .

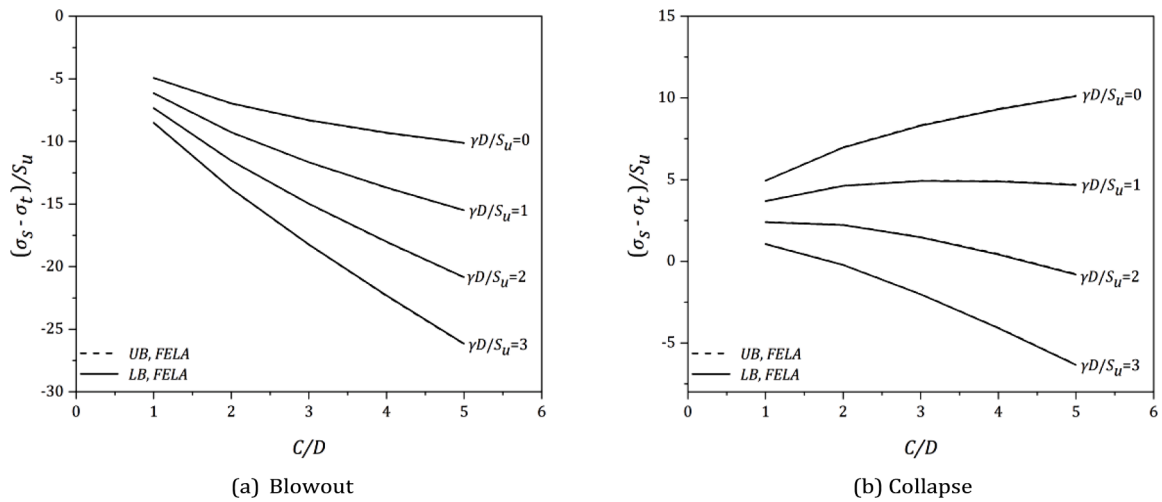


Fig. 11.  $(\sigma_s - \sigma_t)/S_u$  vs  $(C/D)$  for various  $(\gamma D/S_u) - B/D = 1$ .

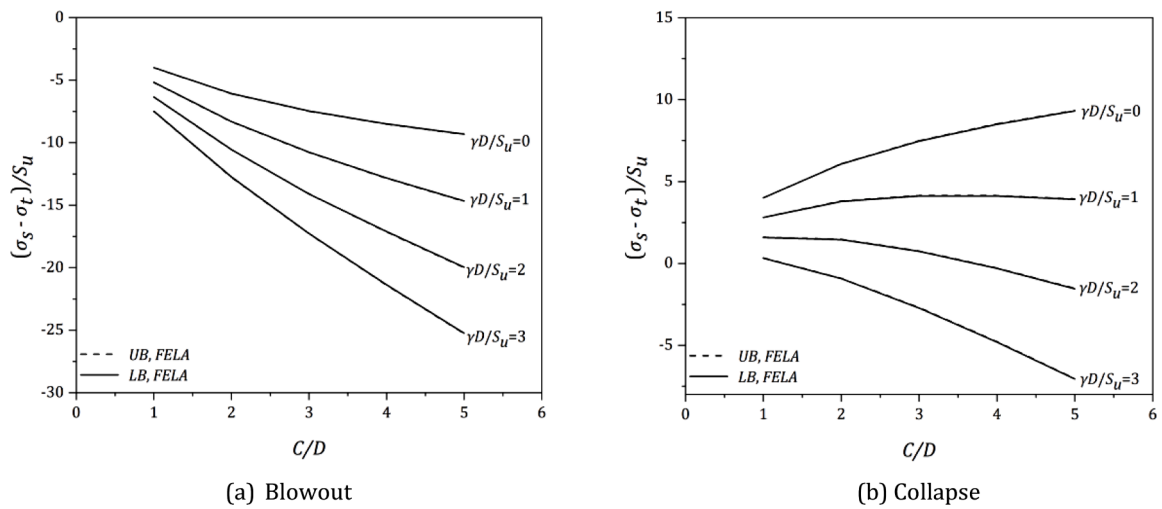


Fig. 12.  $(\sigma_s - \sigma_t)/S_u$  vs  $(C/D)$  for various  $(\gamma D/S_u) - B/D = 1.33$ .

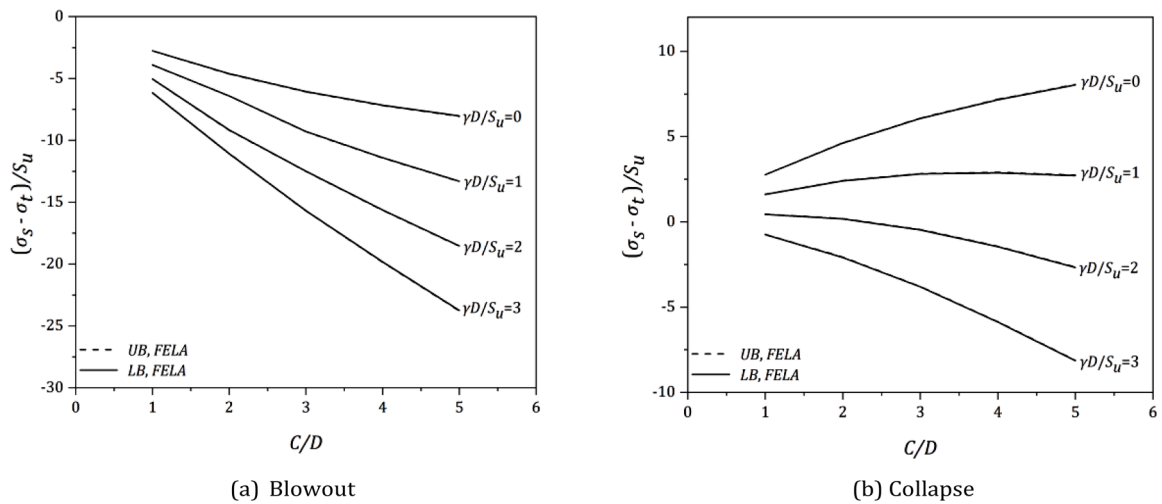


Fig. 13.  $(\sigma_s - \sigma_t)/S_u$  vs  $(C/D)$  for various  $(\gamma D/S_u) - B/D = 2$ .

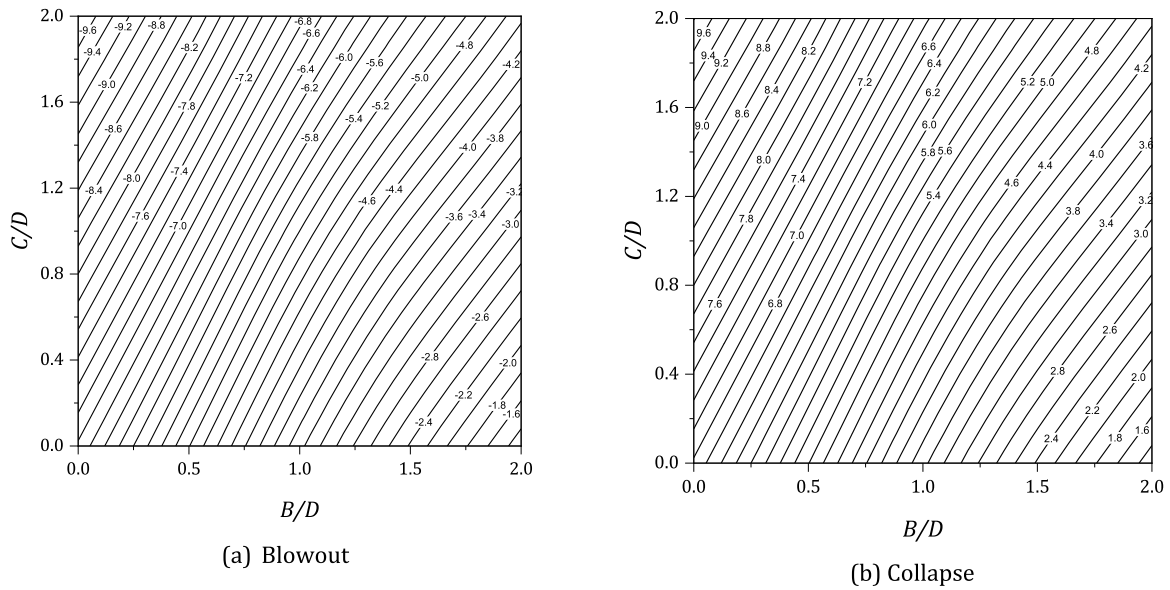


Fig. 14. Design charts for  $\gamma D/S_u = 0$ .

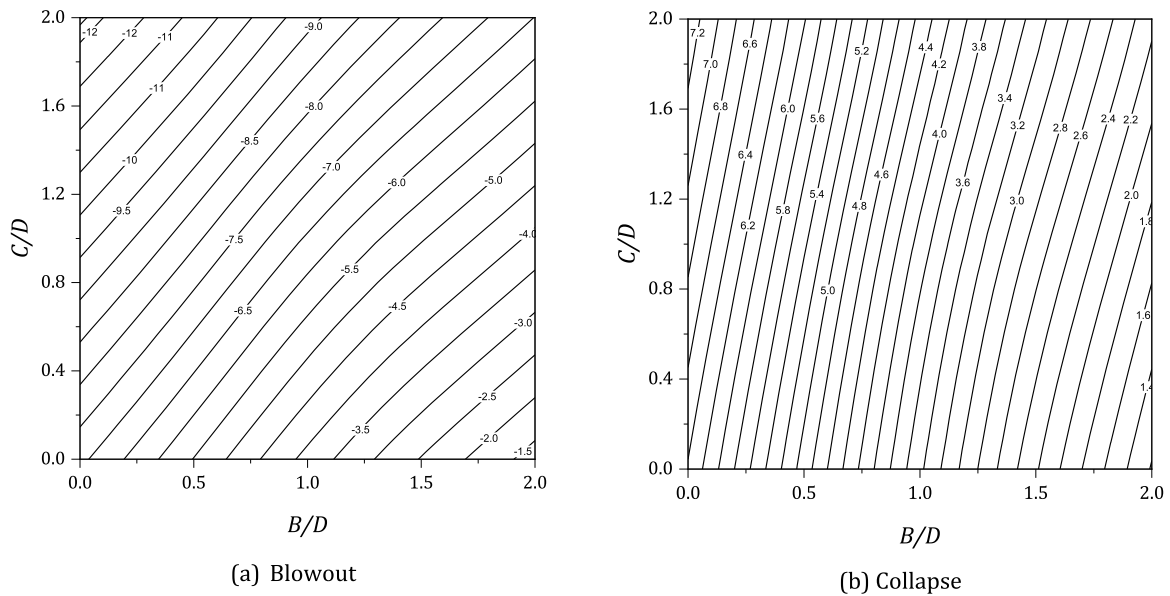


Fig. 15. Design charts for  $\gamma D/S_u = 1$ .

and more useful in this aspect when compared with the stability number stated in Brom and Bennermark (1967). Therefore, the critical pressure ratio ( $PR$ ) in Eq. (3) is used for a wide range of dimensionless parameters in this study. For both blowout and collapse scenarios, a range of depth ratios ( $C/D = 1-5$ ), width-to-height ratios ( $B/D = 0.5-2$ ), and shear strength ratios ( $\gamma D/S_u = 0-3$ ) are explored. The goal is to calculate, using a set of input values ( $C, D, B, \sigma_s, \gamma$ , and  $S_u$ ), the lower and upper bound limits of the critical supporting pressure ( $\sigma_c$ ). To determine the critical pressure ratio ( $PR$ ), the obtained ( $\sigma_c$ ) values from the numerical studies are substituted into Eq. (3).

### 3. Method of analysis

The Finite Element Limit Analysis ( $FELA$ ) discretizes the problem domain into elements and then applies the bound theorems to reach a resolution through an optimization process. These formulations use the same concept of discretizing a domain to generate solutions, with large

optimization problems produced by both upper-bound and lower-bound finite-element formulations that can be resolved using linear or nonlinear programming techniques. The  $FELA$  method can reduce the computational time dramatically in solving stability problems using computers. These have been extensively discussed by Sloan (2013).

The proposed axisymmetric sinkhole problems could be solved by using Optum G2, a finite element software for solving various geotechnical stability problems. The software provides different features to model the details of sinkhole analysis, and repetitive procedures are adopted in different conditions and geometries (Optum CE, 2021).

For the axisymmetric condition, the axial symmetry line at the left of the domain is chosen as the problem's centre line (see Figs. 3 and 4). To form an ellipsoidal cavity, the cavity is modelled as ellipses in 2D under an axially symmetric condition. The critical step for axisymmetric analysis is the setup of boundary support conditions. To reflect the axisymmetric requirement, only vertical movement is permitted at the left-hand side (centreline) of the model. The condition is the same as for

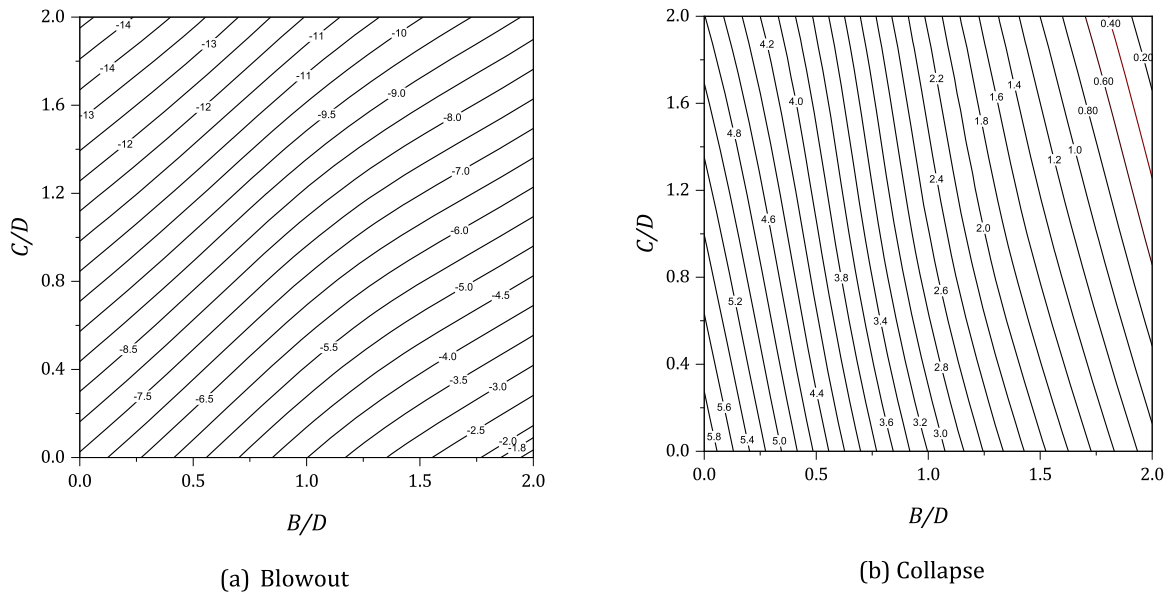


Fig. 16. Design charts for  $\gamma D/S_u = 2$ .

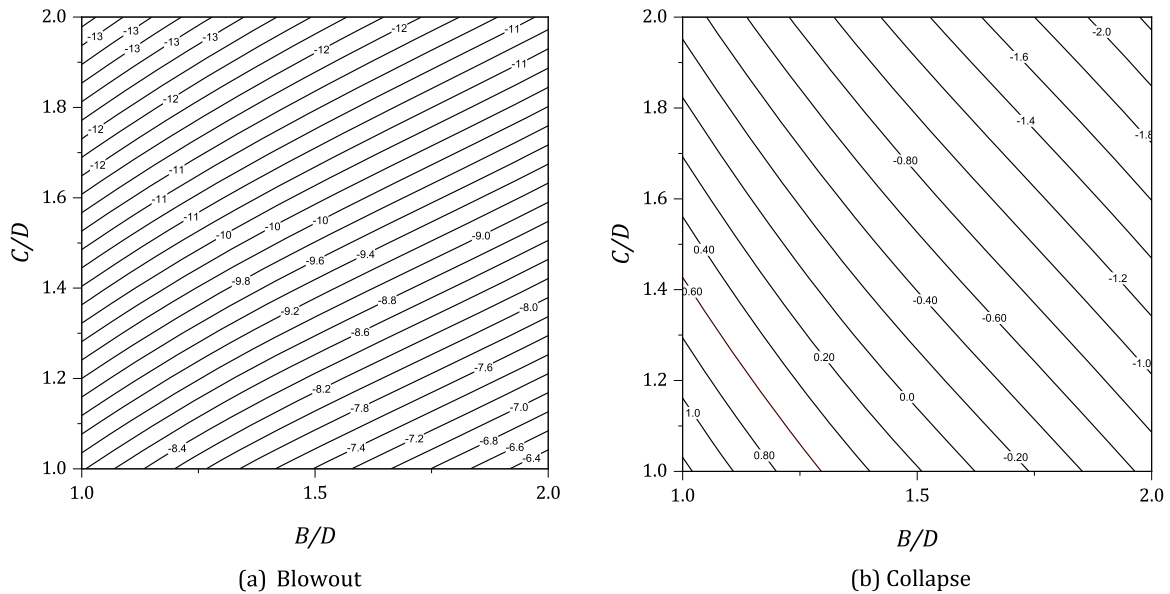


Fig. 17. Design charts for  $\gamma D/S_u = 3$ .

the right-side boundary's far side. Movements in both the vertical and horizontal directions are prohibited at the model's bottom boundary. It should be noted that the domain's size was set to be sufficiently large to make sure that the plastic zone is well located within the proposed domain. It is crucial to note that, in all simulations, the developed velocity field does not cross the right-side boundary.

The loading condition is also important in the modelling. The load multiplier starts at +1 and -1 for blowout and collapse analysis respectively. Afterwards, mesh adaptivity analysis is performed to enhance the accuracy of LB and UB solutions (Ciria et al., 2008). By turning on this adaptivity option, additional elements (based on the magnitude of power dissipation) are added at each iteration step to the sensitive areas with large shear strain gradients to bridge the gap between UB and LB solutions. Mesh adaptivity used for all UB and LB simulations in this paper's analysis is with 5000–10,000 elements used in each iteration step.

#### 4. Results and discussion

Using the FELA analysis stated above, Fig. 5a and 5b show the numerical results for the blowout and collapse pressure ratios ( $PR = (\sigma_s - \sigma_t)/S_u$ ) versus the width-to-height ratio ( $B/D = 0.5$  to 2) for various values of the depth ratio ( $C/D = 1$ –5) of a weightless soil  $\gamma D/S_u = 0$ .

Note that both UB and LB are presented in the figures. Numerical results have shown that all blowout results have negative values of pressure ratios ( $PR = (\sigma_s - \sigma_t)/S_u$ ). A negative  $PR$  value indicates that the compressive normal supporting pressure ( $\sigma_t$ ) is greater than the compressive surcharge pressure ( $\sigma_s$ ). This is because for a blowout failure to occur, ( $\sigma_t$ ) must be greater than  $(\sigma_s + \gamma H)$ . The greater the  $PR$ 's absolute value, the greater the value of  $\sigma_t$ . The absolute value of pressure ratio ( $PR$ ), which increases in the negative axis, increases as  $(B/D)$  increases for all values of  $C/D$ . This is shown in the blowout results in Fig. 5a. As  $(B/D)$  increases, a less critical blowout pressure ( $\sigma_t$ ) is required to produce a blowout failure due to the decrease in the absolute

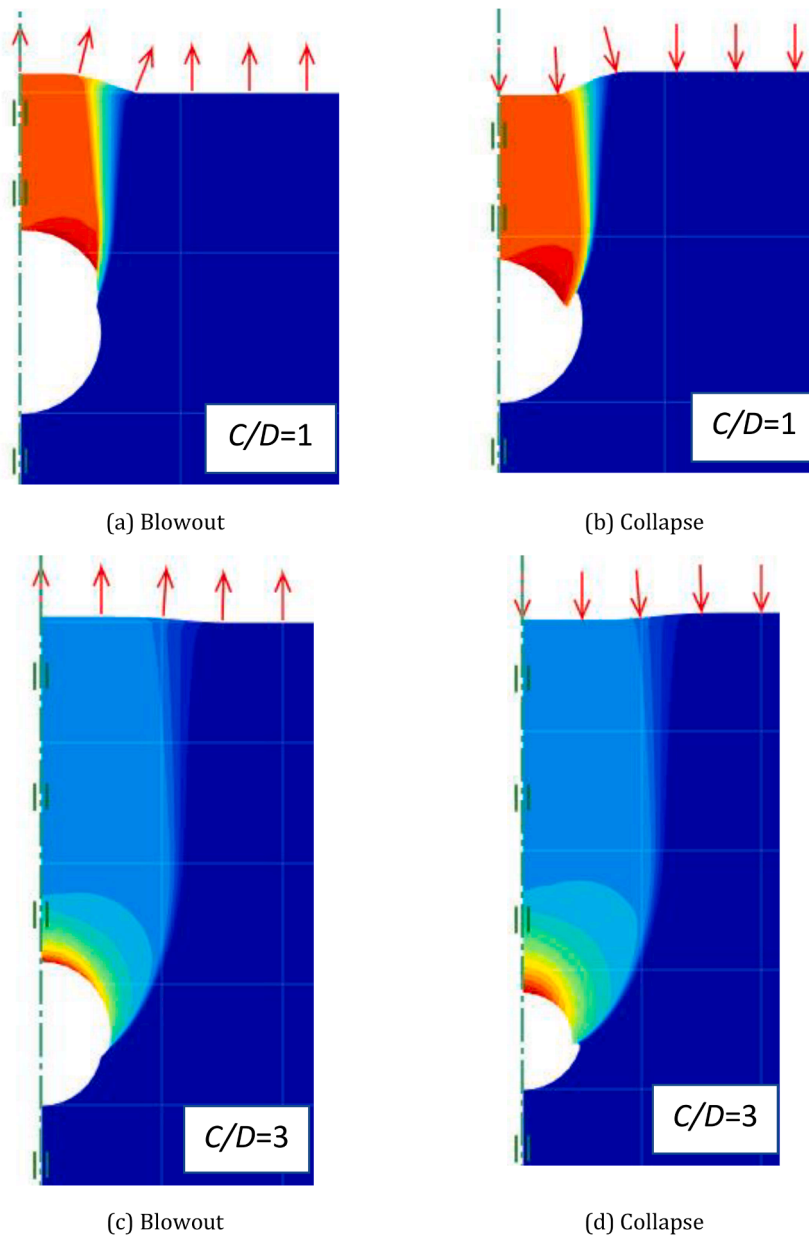


Fig. 18. Absolute velocity ( $|u|$ ) contour plot ( $B/D = 1.0$ ).

value of  $|PR|$ . Additionally, Fig. 5a demonstrates that when the depth ratio ( $C/D$ ) increases, soil stability decreases, which further results in an increase in the absolute value of  $|PR|$ . Similar results are reported in the blowout results for dimensionless shear strength ratios ( $\gamma D/S_u = 1-3$ ) (see Figs. 6a, 7a, and 8a). Note that it takes more blowout pressure ( $\sigma_t$ ) to create a blowout failure as the shear strength ratios ( $\gamma D/S_u$ ) increase when the system is heavier.

In contrast, in the weightless collapse scenario ( $\gamma D/S_u = 0$ ), the  $PR$  values are always positive, which indicates that the compressive surcharge pressure ( $\sigma_s$ ) must be greater than ( $\sigma_t$ ) for a collapse to occur. The numerical results in Fig. 5b demonstrate that, for all depth ratios ( $C/D$ ), the critical pressure ratio ( $PR$ ) decreases as ( $B/D$ ) increases. Additionally, as the depth ratio ( $C/D$ ) increases, the soil stability (i.e., the  $PR$ ) increases. Similar findings are made when looking at the shear strength ratio ( $\gamma D/S_u = 1-3$ ), as demonstrated in Figs. 6b, 7b, and 8b. Greater internal supportive pressure ( $\sigma_t$ ) is required to avoid collapse failure for a heavier system (i.e., larger  $\gamma D/S_u$ ). It is important to note that the value of  $PR$  changes from positive to negative when ( $\gamma D/S_u$ ) increases, showing

that additional internal supportive pressure is required to prevent active failure when the soil is heavier.

The same set of data is used to illustrate the relationship between  $(\sigma_s - \sigma_t)/S_u$  and ( $C/D$ ) for different shear strength ratios ( $\gamma D/S_u$ ). These are shown in Figs. 9–13 for the various values of ( $B/D$ ) respectively. In general, for the blowout scenario, as ( $C/D$ ) increases, the absolute values of the pressure ratio  $PR = (\sigma_s - \sigma_t)/S_u$  also increase (see Figs. 9a, 10a, 11a, 12a, and 13a). This indicates that a larger value of  $\sigma_t$  is required to initiate a blowout failure. It should be noted that as ( $\gamma D/S_u$ ) increases, the rate of increase (in negative  $PR$ ) also increases. The above conclusion is relevant to the blowout situations of various ( $B/D$ ) values. Nevertheless, for the collapse scenario (Figs. 9b, 10b, 11b, 12b, and 13b), both positive and negative values of  $PR$  are possible, as the value of ( $C/D$ ) increases. Note that negative  $PR$  occurs when the values of ( $C/D$ ) and ( $\gamma D/S_u$ ) are larger (such as  $C/D = 5$  and  $\gamma D/S_u = 3$ ). This makes perfect sense because the larger the  $C/D$  and  $\gamma D/S_u$  values, the greater the supporting pressure  $\sigma_t$ .

The bulk of numerical results (blowout and collapse) are presented in

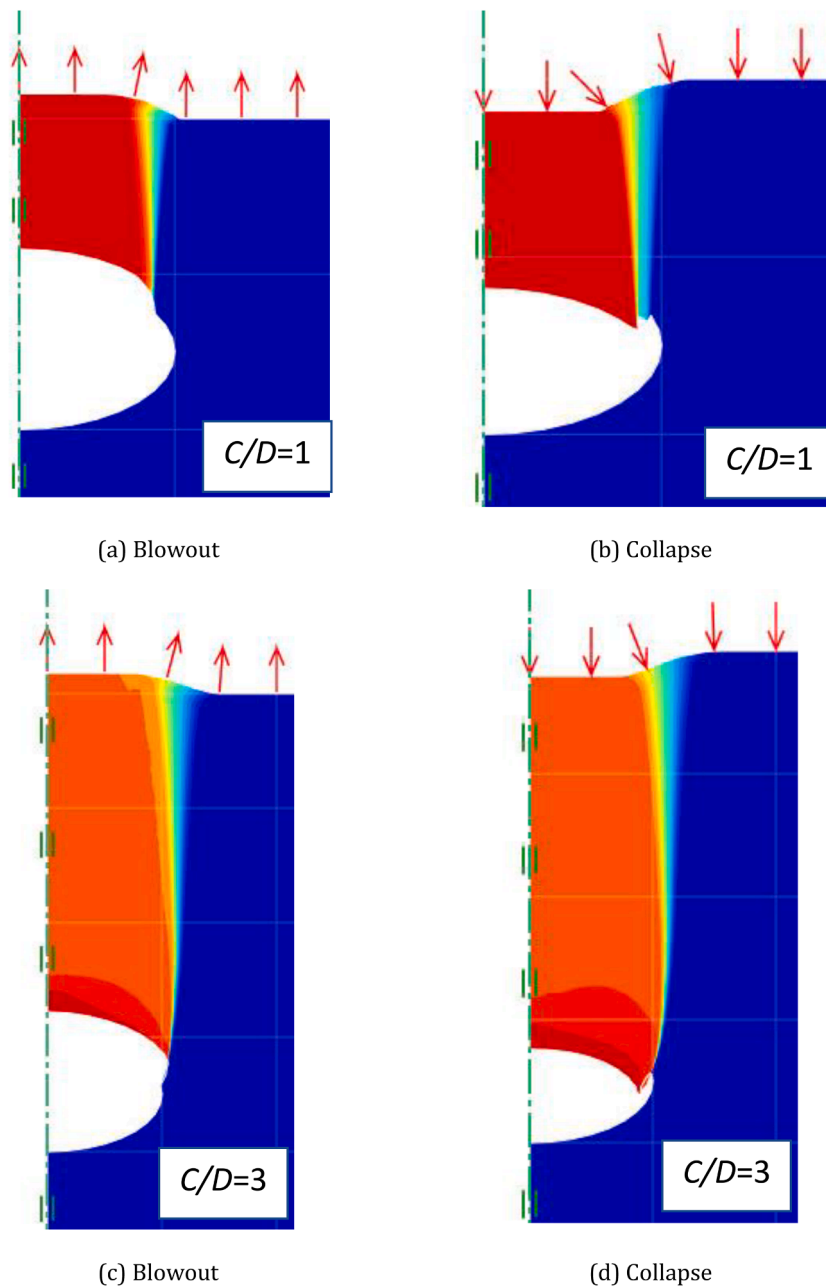


Fig. 19. Absolute velocity ( $|u|$ ) contour plot ( $B/D = 2.0$ ).

Figs. 14–17 for various strength ratios ( $\gamma D/S_u = 0-3$ ) as practical design charts with the width-to-height ( $B/D$ ) and depth ( $C/D$ ) ratios on the axis. The contour values are for the determination of  $PR$ . To obtain a critical pressure ratio ( $PR$ ) from the charts, the designated values of ( $B/D$ ) and ( $C/D$ ) would be needed. An example will be presented in the next section to illustrate how to use these charts.

Figs. 18–19 present contour plots of the absolute velocity fields in different width-to-height ratios ( $B/D = 1$  and  $2$ ). With a shear strength ratio ( $\gamma D/S_u$ ) of  $2$  and two depth ratios ( $C/D$ ) of  $1$  and  $3$ , these plots demonstrate possible blowout and collapse failure modes. Overall, the failure extent in collapse mode is greater than that in the blowout mode and the placement of the initial slip surface points from the inner cavity reinforces the understanding of this observation. In both blowout and collapse scenarios, a chimney-type failure is demonstrated for the shallow depth ratio  $C/D = 1$ , and larger lateral expansions are observed in the deeper case of  $C/D = 3$ . This evidence supports the idea that greater  $\sigma_t$  is required to cause soil blowout failure or to prevent soil

collapse as the value of  $C/D$  is greater. Note that for such a perfectly plasticity soil model, the absolute values of the coloured velocity fields are not real and thus they are not shown in here. They are just for illustrations of possible failure mechanisms.

### 5. Comparison and example

The dimensionless  $PR = (\sigma_s - \sigma_t)/S_u$  values between the current study and those in the prior studies by Augarde et al. (2003) and Keawsawasvong and Ukritchon (2019) are compared in Fig. 20. The comparison is for the scenario of collapse analysis in weightless soil for  $B/D = 1$ . The comparison reveals good agreement for the collapse study between Keawsawasvong and Ukritchon (2019) and the current study. Nevertheless, those of Augarde et al. (2003) are consistently higher than the current results. With the numerical results reported in the comparison, it has increased the confidence in the produced results of the paper. A simple example is given next to explain the use of design charts.

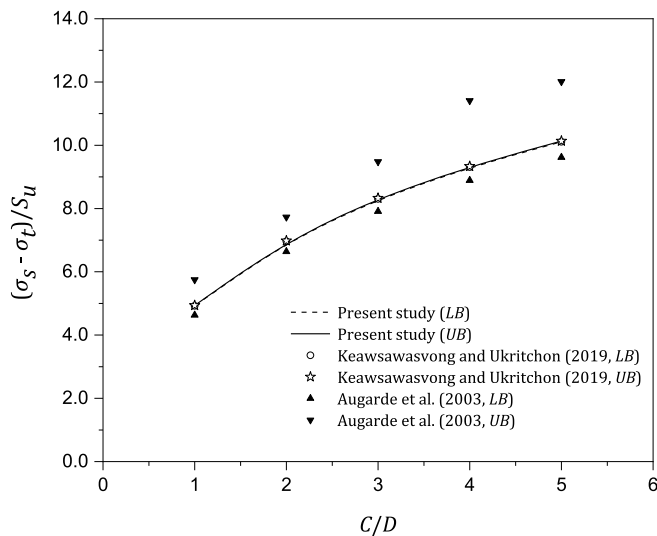


Fig. 20. Comparison of results.

#### Example

Given the following parameters:  $\gamma = 20$  kPa,  $S_u = 40$  kPa,  $\sigma_s = 100$  kPa,  $C = 4$  m,  $D = 2$  m, and  $B = 1$  m, evaluate the ground stability (See Fig. 3 for the notations).

#### Blowout Check

A simple calculation for the problem geometry gives  $C/D = 2$  and  $B/D = 0.5$ . Besides, the strength ratio is given by  $SR = \gamma D/S_u = (20 \times 2/40) = 1$ . From Fig. 15a with  $C/D = 2$  and  $B/D = 0.5$ , the critical pressure ratio is obtained as  $PR = (\sigma_s - \sigma_t)/S_u = -11.25$ . With  $\sigma_s = 100$  kPa and  $S_u = 40$  kPa,  $\sigma_t$  is calculated as 550 kPa, i.e., the critical internal pressure to cause a blowout failure.

#### Collapse Check

For the same problem as in the blowout condition, i.e.,  $C/D = 2$ ,  $B/D = 0.5$ , and  $SR = \gamma D/S_u = 1$ . From Fig. 15b, the critical pressure ratio is  $PR = (\sigma_s - \sigma_t)/S_u = 6.0$  and  $\sigma_t$  is calculated as  $-140$  kPa, given  $\sigma_s = 100$  kPa and  $S_u = 40$  kPa. Since  $\sigma_t$  is negative, it indicates that a pullout pressure is required to induce collapse failure. Theoretically speaking, without such a pullout pressure, a ground collapse failure would not occur.

## 6. Conclusion

The problem of road-related sinkhole stability has been effectively studied in this paper using axisymmetric finite element limit analysis by considering both collapse and blowout failures, which are two typical types of pipeline-related sinkhole failures. For a variety of dimensionless design parameters, including depth ratio, width-to-height ratio, and soil strength ratio, a dimensionless pressure ratio ( $PR$ ) was defined to represent the overall sinkhole stability throughout this paper.

The objective of the study was to determine the rigorous upper and lower solutions of pressure ratios ( $PR$ ) using upper and lower bound solutions. Whilst numerical results were compared with published literature, a series of comprehensive design charts were prepared for practical use. Selected failure mechanisms in blowout and collapse scenarios were also presented and examples demonstrated on how to use the design charts. The proposed approach can be a useful tool for engineers and researchers to evaluate the sinkhole stability of ellipsoidal cavities in various geotechnical conditions. It was recommended that future research can be extended to the seismic stability effects as well as a full 3D finite element limit analysis.

#### Declaration of Competing Interest

The authors declare that they have no known competing financial

interests or personal relationships that could have appeared to influence the work reported in this paper.

#### Data availability

The datasets used and/or analysed during the current study are available from the corresponding author upon reasonable request.

#### Acknowledgement

A part of this paper is based on the research outcomes of the National Asset centre of Excellence (NACOE) Project P164 Optimised and Advanced Geotechnical Solutions. NACOE is a collaborative research agreement between the Queensland Department of Transport and Main Roads (TMR) and the Australian Road Research Board (ARRB). The authors would also like to thank Bishal Chudal for his casual assistance after finishing his postgraduate study.

#### References

- 7news.com.au., 2022, 'Dramatic moment luxury car swallowed by sinkhole in flooding chaos' [online] Available at: <https://7news.com.au/news/wa/watch-dramatic-moment-luxury-car-swallowed-by-sinkhole-in-flooding-chaos-c-8286526> [Accessed 9 Oct. 2022].
- Ali, H., Choi, J., 2019. A review of underground pipeline leakage and sinkhole monitoring methods based on wireless sensor networking. *Sustainability* 11, 4007.
- Augarde, C.E., Lyamin, A.V., Sloan, S.W., 2003. Prediction of undrained sinkhole collapse. *J. Geotech. Geoenviron. Eng.* 129 (3), 197–205.
- Broms, B.B., Bennermark, H., 1967. Stability of clay at vertical openings. *J. Soil Mech. Foundations Division, Proceed. Am. Soc. Civil Eng.* 93, 71–94.
- Ciria, H., Peraire, J., Bonet, J., 2008. Mesh adaptive computation of upper and lower bounds in limit analysis. *Int. J. Numer. Methods Eng.* 75 (8), 899–944.
- Davis, E., Gunn, M., Mair, R., Seneviratne, H., 1980. The stability of shallow tunnels and underground openings in cohesive material. *Geotechnique* 30 (4), 397–416.
- Dutta, P., Bhattacharya, P., 2021. Determination of internal pressure for the stability of dual elliptical tunnels in soft clay. *Geomech. Geoen. Eng.* 16, 67–79.
- Gutiérrez, F., Parise, M., De Waele, J., Jourde, H., 2014. A review on natural and human-induced geohazards and impacts in Karst. *Earth Sci. Rev.* 138, 61–88.
- Indiketiya, S., Jegatheesan, P., Rajeev, P., Kuwano, R., 2019. The influence of pipe embedment material on sinkhole formation due to erosion around defective sewers. *Transp. Geotech.* 19, 110–125.
- Keawsawasvong, S., Likitlersuang, S., 2020. Undrained stability of active trapdoors in two-layered clays. *Underground Space* 10, 1016.
- Keawsawasvong, S., Shiau, J., 2022. Stability of active trapdoors in axisymmetry. *Underground Space* 7 (1), 50–57.
- Keawsawasvong, S., Ukritchon, B., 2019. Undrained stability of a spherical cavity in cohesive soils using finite element limit analysis. *J. Rock Mech. Geotechn. Eng.* 11 (6), 1274–1285.
- OptumCE, 2021. OptumG2. Optum Computational Engineering, Copenhagen, Denmark [online] Available at: <https://optumce.com/> [Accessed 9 Dec. 2022].
- San Francisco Chronicle, 2022, 'Water main break in S.F.'s Richmond district causes sinkhole' [online] Available at: <https://www.sfchronicle.com/sf/article/Water-main-break-in-S-F-s-Richmond-District-17486865.php> [Accessed 9 Oct. 2022].
- Shiau, J., Chudal, Bishal, Mahalingasivam, Kiritharan, Keawsawasvong, Suraparb, 2021b. Pipeline burst-related ground stability in blowout condition. *Transport. Geotechn.* 29, 100587.
- Shiau, J., Chudal, Bishal, Mahalingasivam, Kiritharan, Keawsawasvong, Suraparb, 2022a. Pipeline burst-related soil stability in collapse condition. *J. Pipeline Syst. Eng. Pract.* 3, 04022019.
- Shiau, J., Chudal, Bishal, Mahalingasivam, Kiritharan, Keawsawasvong, Suraparb, Seehavong, S., 2021a. Sinkhole stability in elliptical cavity under collapse and blowout conditions. *Geosciences (Basel)* 11, 421.
- Shiau, J., Lee, Ji-Sung, Al-Asadi, Fadhil, 2021c. Three-dimensional stability analysis of active and passive trapdoors. *Tunnelling Underground Space Technol.* 107, 103635.
- Shiau, J., Mirza, HassanMohammad, 2020. Undrained stability of active and passive trapdoors. *Geotechnol. Res.* 7 (1), 40–48.
- Shiau, J., Mirza, HassanMohammad, 2021. Numerical investigation of undrained trapdoors in three dimensions. *Int. J. Geosynth. Ground Eng.* 7, 30.
- Shiau, J., Suraparb, Keawsawasvong, Lee, Ji-Sung, 2022b. Three-dimensional stability investigation of trapdoors in collapse and blowout conditions. *Int. J. Geomech.* 22, 04022007.
- Shiau, J., Suraparb, Keawsawasvong, Lee, Ji-Sung, 2022c. Three-dimensional circular trapdoor stability. *Transp. Infrastruct. Geotech.* 9, 173–184.
- Sloan, S., 2013. Geotechnical stability analysis. *Géotechnique* 63 (7), 531–571.
- Sloan, S.W., 1988a. A steepest edge active set algorithm for solving sparse linear programming problems. *Int. J. Numer. Methods Eng.* 26 (12), 2671–2685.
- Sloan, S.W., 1988b. Lower bound limit analysis using finite elements and linear programming. *Int. J. Numer. Anal. Methods Geomech.* 12 (1), 61–77.

- Terzaghi, K., 1936. Stress distribution in dry and in saturated sand above a yielding trapdoor. In: *International Conference of Soil Mechanics*, 1. Harvard University, Cambridge, pp. 307–311.
- The Watchers, 2022, 'Massive sinkhole in Chile among the deepest in the world' [online]. Available at: <https://watchers.news/2022/08/07/massive-sinkhole-in-chile-among-the-deepest-in-the-world/> [Accessed 9 Oct. 2022].
- Ukritchon, B., Yoang, S., Keawsawasvong, S., 2019. Three-dimensional stability analysis of the collapse pressure on flexible pavements over rectangular trapdoors. *Transport. Geotech.* 21, 100277 art. no.
- www.9news.com.au, 2022, 'Residents forced to use toilets at local shops after Sydney sinkhole cuts off water supply' [online], Available at: <https://www.9news.com.au/national/burwood-sinkhole-parramatta-road-westconnex-tunnel/a4b27f0a-8c96-46de-a4f7-587b59820118> [Accessed 9 Oct. 2022].
- www.9news.com.au, 2022, 'Australian tourist remains in serious condition after falling in Rotorua sinkhole' [online], Available at: <https://www.9news.com.au/national/australian-tourist-in-serious-condition-after-falling-in-rotorua-sinkhole/60f6a24c-afc0-4e23-8a0d-448cee222819> [Accessed 7 Oct. 2022].
- www.9news.com.au., 2022, 'Pit of hell opened up: the sinkhole opened in the middle of the villa Nueva's main thoroughfare' [online], Available at: <https://www.9news.com.au/world/sinkholes-from-australia-around-the-world-in-pictures/5120b38e-bbc7-4f66-acb0-97a14d96bc93> [Accessed 9 Oct. 2022].
- www.brisbanetimes.com.au., 2022, 'Major sinkhole opens up on Gympie rd in Brisbane after flooding.' [online], Available at: <https://www.brisbanetimes.com.au/national/queensland/major-sinkhole-opens-up-on-gympie-rd-in-brisbane-after-flooding-20220319-p5a62x.html> [Accessed 10 Oct. 2022].
- Yang, F., Sun, X., Zou, J., Zheng, X., 2019. Analysis of an elliptical tunnel affected by surcharge loading. *Proc. Inst. Civ. Eng.-Geotech. Eng.* 172, 312–319.
- Zhang, F., Gao, Y.F., Wu, Y.X., Zhang, N., 2018. Upper-bound solutions for face stability of circular tunnels in undrained clays. *Geotechnique* 68 (1), 76–85.